Final Draft
of the original manuscript:

Hardian, R.; Pistidda, C.; Chaudhary, A.-L.; Capurso, G.; Gizer, G.; Cao, H.;
Milanese, C.; Girella, A.; Santoru, A.; Yigit, D.; Dieringa, H.; Kainer, K.U.;
Klassen, T.; Dornheim, M.:

Waste Mg-Al based alloys for hydrogen storage

Waste Mg-Al based alloys for hydrogen storage

R. Hardian,[a] C. Pistidda,[a]* A.-L. Chaudhary,[a] G. Capurso,[a] G. Gizer,[a] H. Cao,[a] C. Milanese,[b]
A. Girella,[b] A. Santoru,[a] D. Yigit,[c] H. Dieringa, [e] K. U. Kainer,[e] T. Klassen,[a,d] M. Dornheim.[a]

[a]Institute of Materials Research, Materials Technology, Helmholtz-Zentrum Geesthacht
GmbH, Max-Planck-Straße 1, D-21502 Geesthacht, Germany.
[b]Pavia Hydrogen Lab, CSGI & Università di Pavia, Dipartimento di Chimica, Sezione di
Chimica Fisica, Viale Taramelli, 16, 27100 Pavia, Italy
[c]Zoz Group, Wenden, Germany
[d]Department of Mechanical Engineering, Helmut Schmidt University, Holstenhofweg 85,
Hamburg, Germany
[e]Magnesium Innovation Centre-MagIC, Institute for Materials Research, Helmholtz-Zentrum
Geesthacht, Max-Planck-Straße 1, D-21502 Geesthacht, Germany

Email: claudio.pistidda@hzg.de

Abstract

Magnesium has been studied as a potential hydrogen storage material for several decades
because of its relatively high hydrogen storage capacity, fast sorption kinetics (when doped
with transition metal based additives), and abundance. This research aims to study the
possibility to use waste magnesium alloys to produce good quality MgH_2. The production costs
of hydrogen storage materials is still one of the major barriers disabling scale up for mobile or
stationary application. The recycling of magnesium-based waste to produce magnesium
hydride will significantly contribute to the cost reduction of this material. This study focuses
on the effect of different parameters such as the addition of graphite and/or Nb_2O_5 as well as
the effect of milling time on the material hydrogenation/de-hydrogenation performances. In
addition, morphology and microstructural features are also evaluated for all the investigated
materials.

1. Introduction

The continuous growth of the world population combined with the increased awareness toward
environmental and health issues connected to the massive use of fossil fuels lead to an increase

in the demand for a clean and sustainable energy solution. In this scenario, nuclear power cannot be considered a reliable and safe energy source for the long-term period. The problems arising from the difficulties to store the waste materials and the accident in Fukushima (Japan) seriously weakened the plans of many governments to invest in this technology. In view of a long-term energy provision solution, the only available alternative to the production of energy from fossil fuels is to harvest it from renewable energy sources, such as sunlight, wind, tide and biomasses. The transition from fossil fuels to sustainable energy is extremely challenging from the technological point of view. In fact, a complete exploitation of renewable energy sources is difficult because of their intermittent nature and uneven availability on Earth. Therefore, an energy storage media is needed. In this regard, because of its high energy density per mass and environmental friendliness, hydrogen is widely considered as a key element for a potential energy solution.[1, 2] The possibility to produce hydrogen utilizing renewable sources and to store energy in it presents multiple advantages. On the one hand, energy will be harvested and stored nearly without the production of harmful pollutants, and on the other hand the security of energy supply will be granted. In addition, the implementation of hydrogen as "energy carrier" is expected to result in an effective and synergic utilization of the renewable energy sources. In order to achieve these aims, hydrogen storage technology is a key roadblock towards the use of H_2 as an energy carrier. Hydrogen is usually stored in three main forms: (i) as highly pressurized gas at 350 and 700 bar, (ii) liquefied hydrogen at -253 °C and (iii) in solid state form chemically bonded. Among these methods, the storage of hydrogen in solid state as metal hydrides appears to be the most attractive alternative both from the safety and the volumetric energy density points of view.[3, 4]

Among other metal hydrides, because of its high energy densities (9 MJ/kg Mg) and good reversibility (when doped with transition metal based additives),[5] magnesium hydride has been the subject of intensive studies aimed at assessing its potential as a hydrogen storage system alone, [6-17] in combination with alloying species (dual-tuning approach)[18-26] and in combination with other hydrides (reactive hydride composite approach i.e. RHC).[27-47] Beside the material properties, the production cost of materials for hydrogen storage is a major barrier to overcome in order to consider these materials suitable for large scale applications.[48] The utilization of magnesium-based wastes to produce magnesium hydride will significantly contribute to the cost reduction of this material.

Following our previous work related to the use of waste magnesium [49], this study shows the possibility of producing high quality/high performance MgH_2 starting from a mixture of Mg-

Al waste alloys. The hydrogenation/de-hydrogenation properties of the starting material and of the same after milling process are investigated via volumetric measurements. A detailed account on the effect of the milling process on the microstructural and kinetic properties of the obtained material is given. For targeted batches of material the effect of Nb_2O_5 on their hydrogenation/de-hydrogenation properties is also investigated.

2. Experimental

2.1. Sample preparation

The as-received material consisted of a mixture of waste Mg-Al based alloys obtained from the in-house technical workshop at the Helmholtz-Zentrum Geesthacht in shape of shavings. Before starting this work, the material was stored in air for several months.

In this research work, the material was prepared following three different routes.

In the first preparation route (R1), the received material was milled using a Simoloyer CM08 industrial mill from Zoz GmbH for 20, 60, and 120 minutes with the addition of 10 wt% of graphite. In the second preparation route (R2), the received material was milled using the same CM08 ball-mill for 120 minutes with the addition of 5 wt% of graphite. In the third preparation route (R3), the as-received material was milled using again the CM08 mill for 20, 60, and 120 minutes with the addition of 10 wt% of graphite and 5 wt% of Nb_2O_5. The complete milling conditions are reported in Table 1 and the summary of the prepared samples is presented in Table 2.

Table 1. Process parameters used during milling with the Simoloyer CM08 mill.

Process parameters	R1	R2	R3
Balls material	100Cr6	100Cr6	100Cr6
Balls diameter	5 mm	5 mm	5 mm
Total mass of balls	8000 grams	8000 grams	8000 grams
Mass of as-received Mg shavings	350 grams	350 grams	350 grams
Mass of graphite	35 grams (10 wt%)	17 grams (5 wt%)	35 grams (10 wt%)
Mass of Nb_2O_5	-	-	17.5 grams (5 wt%)
BPR	1:20	1:20	1:20
Pre-mixing	150 rpm / 1 min + 300 rpm / 2 min	150 rpm / 1 min + 300 rpm / 2 min	150 rpm / 1 min + 300 rpm / 2 min
Processing time	120 min	120 min	120 min
Cycle processing	700 rpm/30 s – 300 rpm / 30 s	700 rpm/30 s – 300 rpm / 30 s	700 rpm/30 s – 300 rpm / 30 s
Sampling	20 min, 60 min, 120 min	120 min	20 min, 60 min, 120 min
Discharging	after 120 min : 150 rpm/6 min + 30x {200 rpm/15 s- 250 rpm/10 s} + 300 rpm/1 min + 350 rpm/2 min + 400 rpm/1 min + 500 rpm/2 min	after 120 min : 150 rpm/6 min + 30x {200 rpm/15 s- 250 rpm/10 s} + 300 rpm/1 min + 350 rpm/2 min + 400 rpm/1 min + 500 rpm/2 min	after 120 min : 150 rpm/6 min + 30x {200 rpm/15 s- 250 rpm/10s} + 300 rpm/1 min + 350 rpm/2 min + 400 rpm/1 min + 500 rpm/2 min

Table 2. Summary of the studied samples.

	Milling time (min)	Identity
As-received	0	as received
R1 (with 10 wt% graphite)	20	R1-20
	60	R1-60
	120	R1-120
R2 (with 5 wt% graphite)	120	R2-120
R3 (with 10 wt.% graphite and 5 wt% Nb_2O_5)	20	R3-20
	60	R3-60
	120	R3-120

2.2. Material characterization

The morphology and local composition of the material were studied by scanning electron microscopy with energy dispersive X-ray spectroscopy (SEM/EDX), using an EvoMA10 microscope (Zeiss, Germany) equipped with a LaB_6 filament and with a XMax 50mm^2 EDX probe (Oxford, UK). The calibration for the elemental analysis is done with Co standard. To avoid oxidation during the material handling, a special home-made air tight sample holder was used to transfer the milled materials from an argon filled glove box (O_2 and H_2 levels $\leq$ 1 ppm) to the SEM machine. *Ex situ* powder x-ray diffraction (XRD) analyses were carried out with a Siemens D5000 X-ray diffractometer, using Cu Kα radiation ($\lambda = 1.54056$ Å). The powder was

spread onto a silicon single crystal plate and sealed in the glove box with an airtight hood transparent to the X-rays. The material composition and crystallite size of the material was evaluated using the DIFFRAC^{plus} TOPAS 4.2 software (Bruker, Germany). The internal stress evolution of material was calculated from the strain values taking into consideration the Young's modulus of these Mg alloys that is roughly 45 GPa.[50] The material hydrogenation/de-hydrogenation properties were evaluated using a volumetric instrument HERA system (HERA, Quebec, Canada) and a PCTPro-2000 (Setaram, France). For each analysis roughly 150 mg of material were loaded in an especially designed stainless steel sample holder inside an argon filled glovebox (O_2 and H_2 levels ≤ 1 ppm). The hydrogenation processes were carried out at 350 °C under a hydrogen pressure of 13 bar for 1 hour, whereas the de-hydrogenation processes were performed at 350 °C and 0.5 bar hydrogen pressure for 30 minutes. The de-hydrogenation process of the previously hydrogenated material was investigated by differential thermal analysis (DTA) using a DTA NetzschSTA409 equipment (Germany) located in a dedicated glove box under argon atmosphere (O_2 and H_2 levels ≤ 1 ppm). For each DTA analysis an amount of powder of about 15 mg was loaded in an alumina (Al_2O_3) crucible. The material was heated from room temperature (RT) up to 400 °C with heating rates of 2 °C/min, 3 °C/min, 5 °C/min, and 10 °C/min in a constant argon flow of 50 mL/min.

3. Results

The SEM micrographs of the materials as-received and after the milling process are reported in Figure 1-4. The as-received material is in the form of flat ribbons often curled, which have different sizes and dimensions in the range between several hundred micrometers to millimeters (Figure 1: left). Mostly the size and shape of the as-received materials remains unchanged after attempting to hydrogenate it (Figure 1: right).
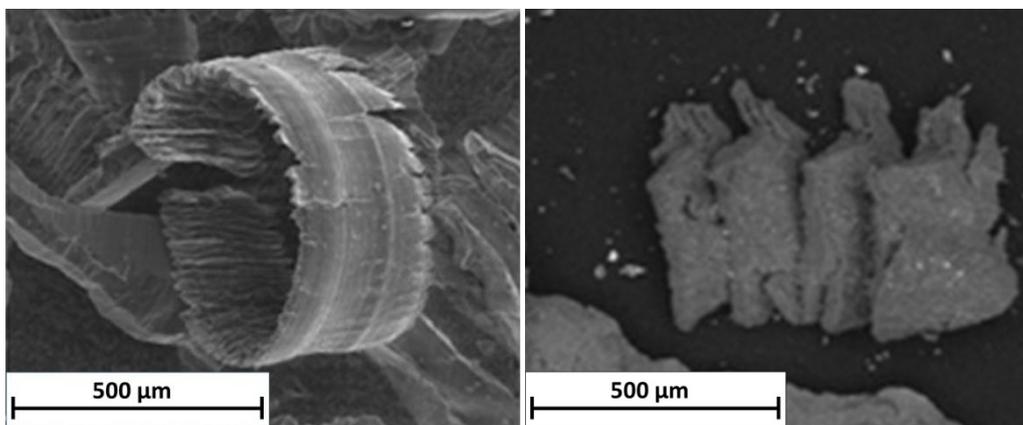
Figure 1. SEM images of the as-received material, before (left) and after hydrogenation (right).

The material R1-20 shows an average particle size of about 600 μm (Figure 2). For R1-60, the mean particle size lays in the range of 50–200 μm and, subsequently, the sample becomes finally powdered with a particle size of about 20 μm after a milling time of 120 minutes (R1-120). The SEM image of R2-120 is presented in Figure 3. Also in this case, as for R1-120, the material particle size after milling is of about 20 μm.
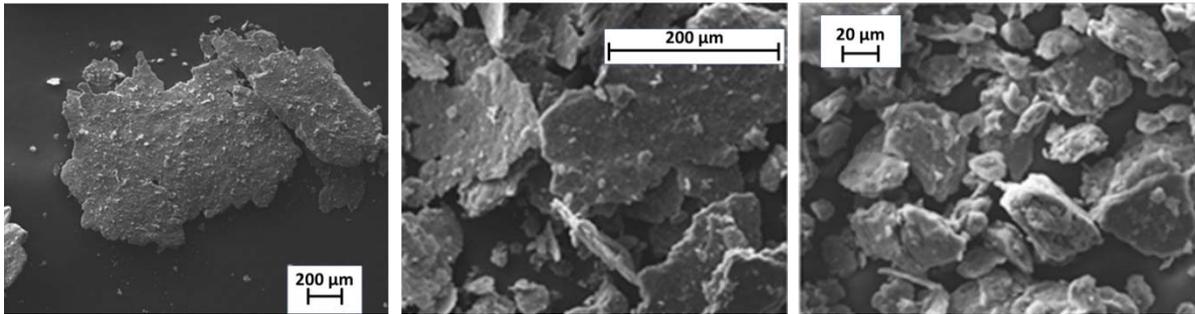
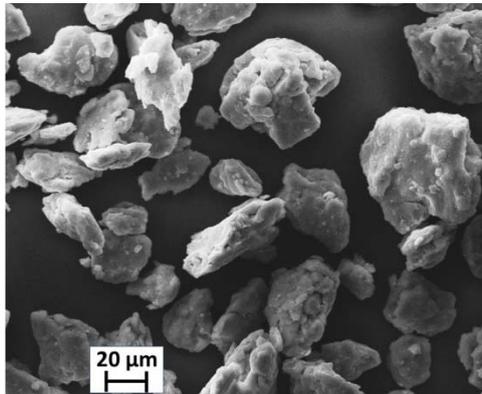

Figure 2. SEM images of samples R1-20, R1-60, and R1-120.

Figure 3. SEM image of sample R2-120.

In order to investigate the effects of the milling time on the distribution of Nb_2O_5, EDX mapping was performed on the samples in series R3 (R3-20, R3-60, and R3-120) and the results are presented in Figure 4. The red circles were made only as guidance to help indicating one position where Nb was identified, so that the whole Nb distribution obtained by the EDX mapping can be easily compared with the corresponding SEM images. EDX mapping from SEM images shows that at a short milling time (R3-20) the catalyst seems to be agglomerated and not well distributed, located only on the outer surface of the milled materials. By increasing the milling time up to 60 minutes (R3-60), the catalyst appears better distributed. There are

fewer amounts of catalyst particles observed on the surface of the material R3-60 in comparison to R3-20. Increasing the milling time to 120 minutes (R3-120) the catalyst distribution improves even further. In fact, it appears as if the Nb_2O_5 particles are mostly embedded in the bulk of the material since just few particles are clearly visible on the surface of the materials.
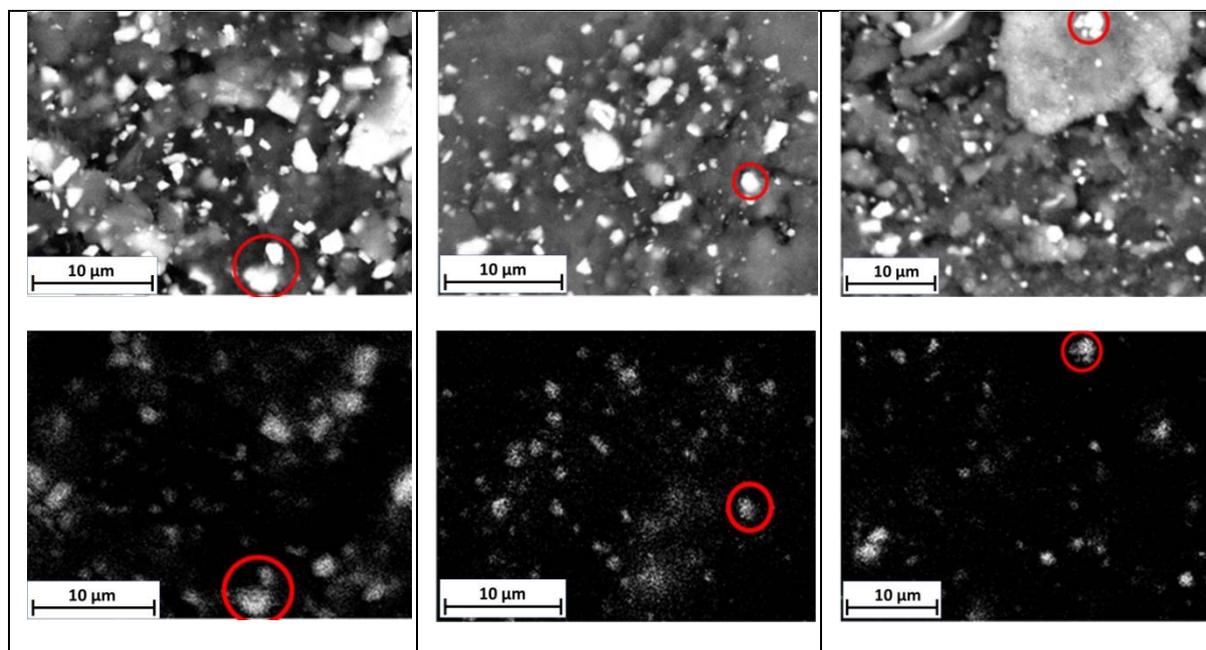

Figure 4. SEM images (top row) and EDX analysis (bottom row) of samples R3-20 (left column), R3-60 (central column), and R3-120 (right column).

Constituent crystalline phases of as-received materials and of milled samples were investigated using XRD and the results are reported in Figure 5. As it can be observed, the as-received material and the material milled without Nb_2O_5 are composed of Mg and Al (Figure 5 left) whereas in the samples milled with Nb_2O_5 the reflections of Nb_2O_5 are also visible in the 2 theta range $24°–27°$ (Figure 5 right). Based on the Rietveld analysis of as received material we can estimate the material composition to be roughly 96 wt% Mg and 4 wt% Al. It is interesting to notice that although expected the phase $Al_{12}Mg_{17}$ is not clearly visible in any diffraction pattern. This is most likely due to the small amount of it and to the overlapping of its diffraction peaks with the more intense peaks of Mg. The rest of the elements that were identified in EDX analysis (see SI Figure 1) are not visible because of their small amount and most likely because of nanometric size of particles containing them. Noticeably, despite the fact that the raw material was stored in air for several months prior the utilization in this work, no traces of MgO are observed in any of the investigated samples.
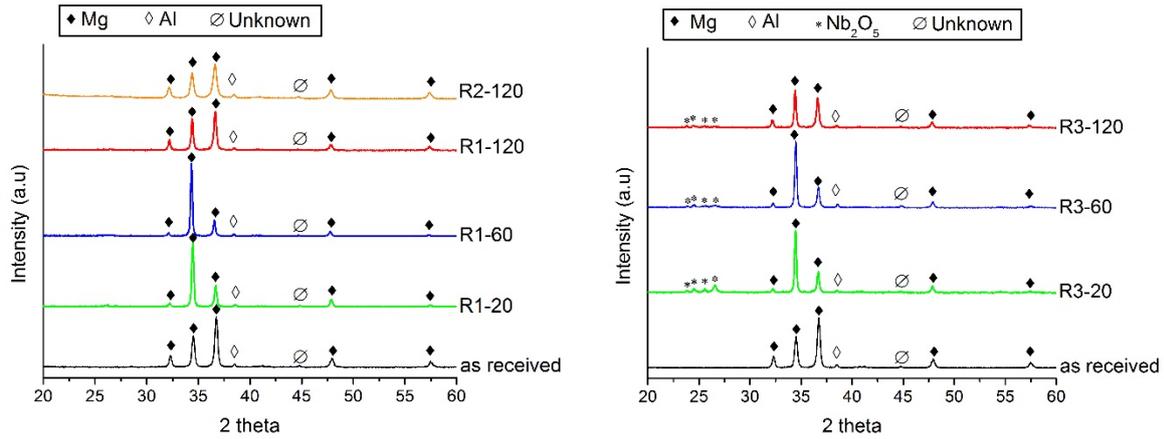
Figure 5. XRD patterns of: material as-received plus R1 series (left) and as-received plus R3 series (right).

The hydrogenation/de-hydrogenation kinetics of all the investigated materials were measured via volumetric technique and the results are reported in Figure 6. The displayed kinetics are those relative to the 3rd hydrogenation/de-hydrogenation cycle. In fact, we consider the first two cycles as necessary for the activation of the material.
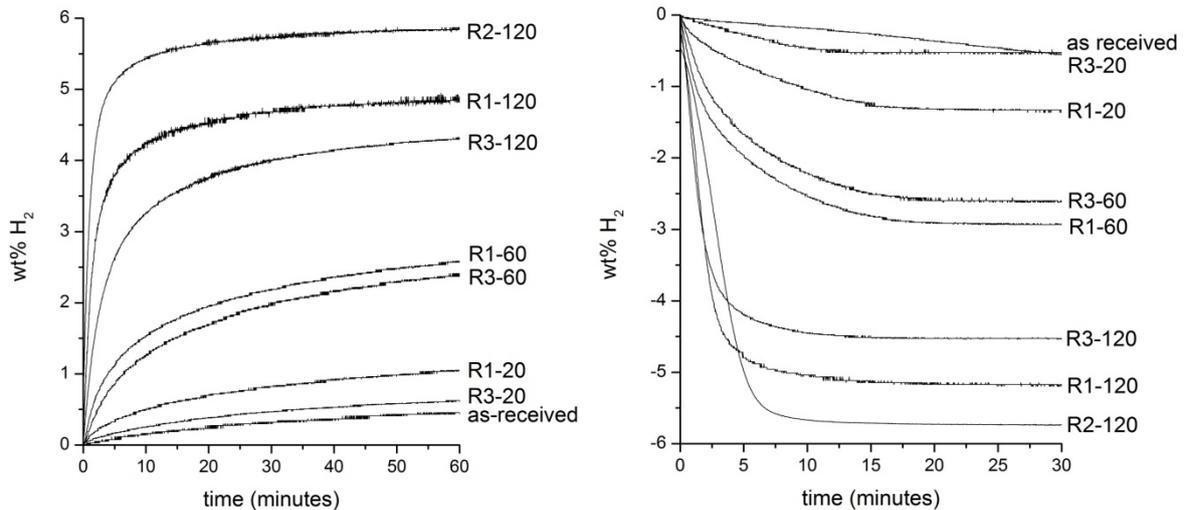

Figure 6. 3rd cycle hydrogenation/de-hydrogenation kinetics for: as-received, R1-20 , R3-20, R1-60, R3-60, R1-120, R3-120, R2-120 samples. Left: hydrogenation; right: de-hydrogenation.

As expected, both hydrogenation and de-hydrogenation reactions take place in a single step. The highest hydrogen capacity measured within a time frame of one hour (~6 wt%) is obtained for the material R2-120. For the material prepared using the same milling conditions but an amount of graphite equal to 10 wt% the capacity decreases to about 4.8 % (R1-120). The addition of 5 wt% of Nb_2O_5 further reduces the maximum hydrogen capacity to 4.3 wt% (R3-

120). Decreasing the milling time from 120 to 60 minutes results in a system which has a medium hydrogen storage capacity of about 2.5 wt% (R1-60). For the material milled under the same condition of R1-60 but with the addition of Nb_2O_5 (R3-60) the hydrogen capacity decreases to 2.3 wt%. Meanwhile, for the materials milled for just 20 minutes, the capacities are less than 1 wt% without or with the catalyst (R1-20 and R3-20, respectively), values not significantly different from the hydrogen capacity measured for the as-received material (0.25 wt%). Interestingly, for equal milling time the kinetic properties of R3 are the same as those of R1.

To understand the reasons of the reduced hydrogen capacity shown by the material milled for 120 minutes (i.e. R1-120, R2-120 and R3-120), the samples obtained after the 3rd hydrogenation/de-hydrogenation cycle were re-hydrogenated and characterized by XRD technique. The obtained results are shown in Figure 7.
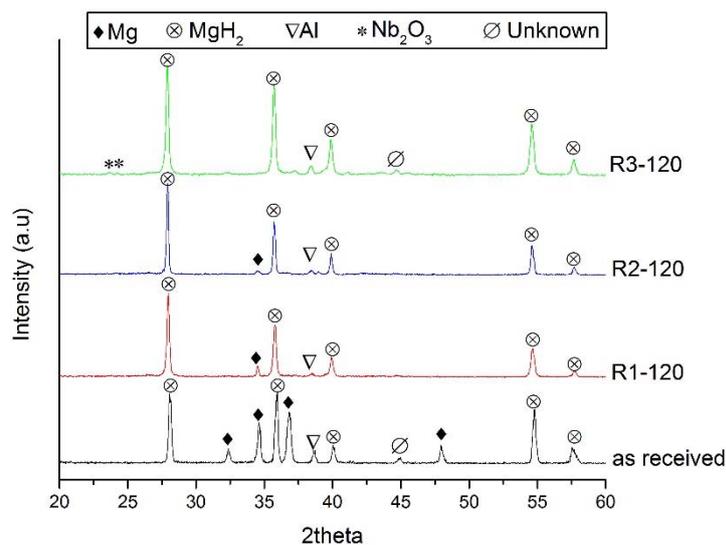

Figure 7. XRD patterns of the materials hydrogenated after the 3rd cycle: as-received, R1-120, R2-120, and R3-120.

As it can be noted, the diffraction peaks of MgH_2 are present in the diffraction patterns of all the investigated samples. However, no peaks attributable to magnesium are visible in the diffraction pattern of hydrogenated R2-120. Meanwhile, the peaks of unreacted magnesium are still clearly visible for the other samples.

In order to determine the activation energy during de-hydrogenation, all hydrogenated samples were characterized using DTA. The heat flow during the temperature increase (from room temperature up to 400 °C) was measured at several heating rates (2, 3, 5, and 10 K/min). The activation energies were then calculated using the Kissinger method. The derived Kissinger plots are presented in Figure 8 and the activation energies of the different materials are tabulated in Table 4.
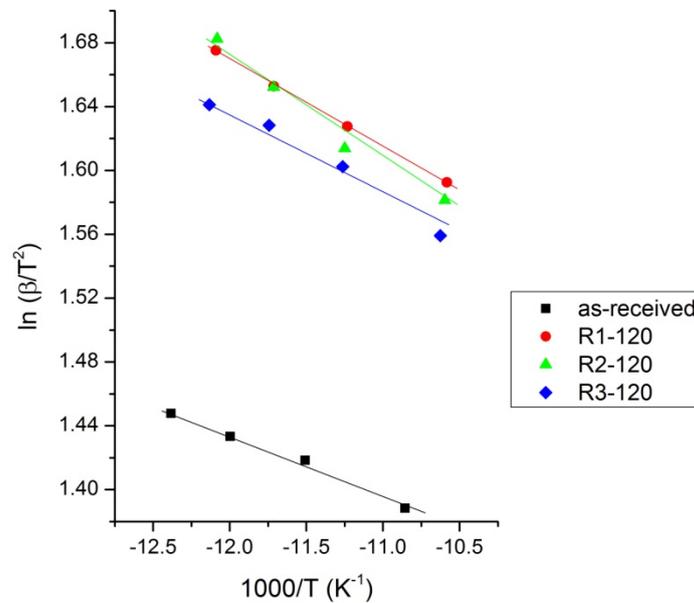

Figure 8. Kissinger plot for: as-received material, R1-120, R2-120, and R3-120.

The as-received material has the highest activation energy for desorption, i.e. 215 kJ/mol. The materials R1-120 and R2-120 have de-hydrogenation activation energies of 154 kJ/mol and 119 kJ/mol, respectively. The activation energy of the sample R3-120 is 148 kJ/mol.

The cycling hydrogenation/de-hydrogenation behaviors of the as-prepared materials are shown in Figures 9-11 for the samples R1, R2 and R3 respectively. The reversible hydrogen storage capacity upon cycling of the investigated samples is relatively stable, except for R1-20. In fact, for this sample the hydrogen storage capacity, which for the 1st cycle is about 0.25 wt%, reaches a maximum value of 0.75wt% in the 4th cycle, before gradually decreasing to 0.35 wt% in the 6th cycle. The samples R1-60 and R1-120 show full reversibility and hydrogen storage capacities of c.a. 3 and 5.2 wt% respectively. The sample R2-120 shows the highest hydrogen storage capacity among the investigated samples (c.a. 6 wt%) and it is fully reversible over the 11 cycles performed within the 20 hours of the volumetric experiment. Finally, all the samples R3 show complete reversibility and hydrogen storage capacity that grow with the increasing of

the milling time. The measured capacities are 1.4 wt%, 2.7wt% and 4.5wt% for R3-20, R3-60 and R3-120 respectively.
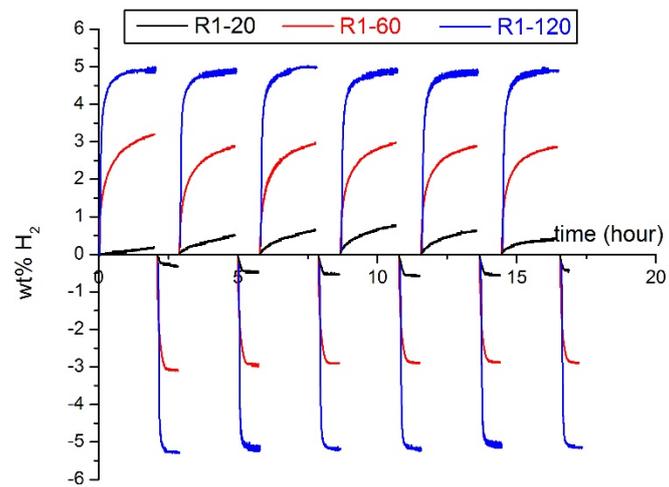

Figure 9. Hydrogenation/de-hydrogenation cycles of R1-20, R1-60, and R1-120.
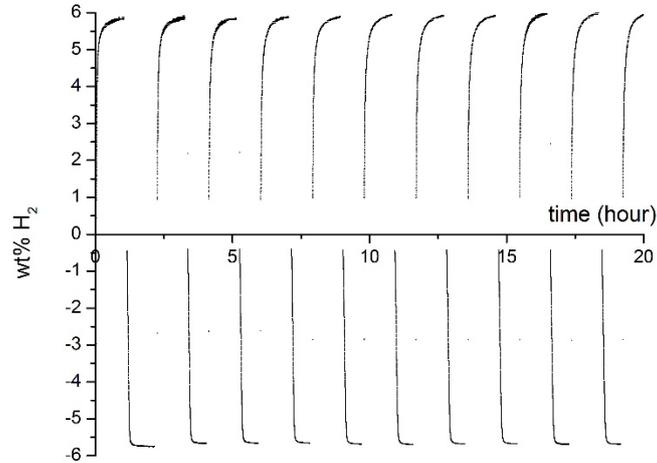

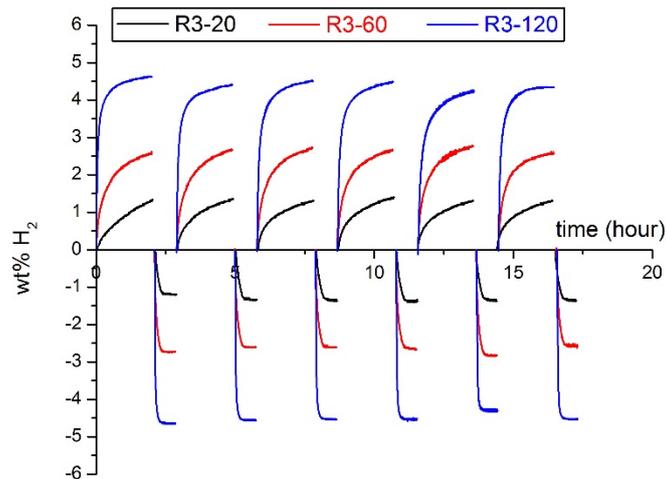Figure 10. Hydrogenation/de-hydrogenation cycles of R2-120.

Figure 11. Hydrogenation/de-hydrogenation cycles of R3-20, R3-60, and R3-120.

4. Discussion

In this work, the possibility to produce high quality/high performance MgH$_2$ starting from mixtures of waste Mg-Al based alloys was studied. The applied ball-milling procedure of the starting material was necessary both to reduce the alloy particles size and to break the MgO/Mg(OH)$_2$ nano-metric layer that always covers the topmost part of Mg and Mg alloy surfaces.[51-61] The reduction of material particle size is of particular importance for two main reasons. In fact, it is well known that in the early stages of the hydrogenation of the magnesium fraction in the alloys, the process is limited by the H$_2$ dissociation on the material surface [10, 14, 62] therefore a larger surface area greatly enhances the rate of the absorption process.[63] Moreover, since the diffusion of H$_2$ trough MgH$_2$ is hindered,[10] reducing the starting dimension of the Mg alloy particles is of primary importance to achieve a full hydrogenation of the material. [13, 14] The addition of graphite as dispersant agent has been necessary to avoid agglomeration and cold-welding phenomena during ball-milling.[64] Interestingly, the addition of 10 rather than 5 wt% of graphite did not change the final particle size of the material. In fact, in both cases after 120 minutes of milling time the average particle size is about 20 μm (Figure 2 and 3). As expected, the different milling time has a clear effect on the hydrogenation/de-hydrogenation properties of the material milled both with a 10 wt% of graphite and with 10 wt% of graphite plus 5 wt% Nb$_2$O$_5$ (R1 and R3 in Figure 6). However, for equal time of milling, the most significant difference between the material milled with 10 wt% of graphite (R1) and that milled with 10 wt% of graphite plus 5 wt% Nb$_2$O$_5$ (R3) is the

overall hydrogen capacity of the system, which is lower for the material containing Nb_2O_5. In fact, when observing the hydrogenation and de-hydrogenation rates measured for the material R1 and R3 during the 3rd hydrogenation/de-hydrogenation cycle at the 80% of conversion, it is visible that for equal time of milling they are practically the same (Table 3). The material R2-120 shows faster hydrogenation rates compared with the samples R1-120 and R3-120 but markedly slower de-hydrogenation rate. For comparison purposes, also the hydrogenation and de-hydrogenation rates of the as received material were measured.

Table 3. 3rd cycle hydrogenation and de-hydrogenation rates at 80% conversion grade.

Sample	Hydrogenation rate (wt %/min)	De-hydrogenation rate (wt %/min)
As-received	1.29	2.31
R1-20	1.37	8.58
R1-60	2.91	9.66
R1-120	12.27	28.27
R2-120	26.85	17.98
R3-20	0.99	7.25
R3-60	4.32	9.37
R3-120	17.89	30.53

An identical trend is observed for the activation energy of de-hydrogenation process of samples as-received, R1-120, R2-120 and R3-120 (Table 4). The values measured for the samples R1-120, and R3-120 are extremely close to each other, i.e. 154 kJ/mol H_2 and 148 kJ/mol H_2 respectively. These values are lower than the one of the as-received material (i.e. 216 kJ/mol H_2) but higher than the one of of R2-120 (i.e. 120 kJ/mol H_2). The activation energy values of R1-120 and R3-120 are in good agreement with those reported in literature by R. Campostrini and R. Schultz for the de-hydrogenation of un-milled commercial MgH_2.

Table 4. Activation energy of de-hydrogenation (kJ/mol) of the materials prepared via different milling conditions plus reference values for un-milled MgH_2.

Sample		Ea (kJ/mol H_2)	Identity
Literature	A	175	MgH_2 powder 96.5% purity [65]
	B	156	MgH_2 powder (95%) [66]
Sample	As-received	215	as-received material after hydrogenation
	R1-120	154	as-received Mg, milled with 10 wt% graphite for 120 min
	R2-120	119	as-received material, milled with 5 wt% graphite for 120 min
	R3-120	148	as-received material, milled with 10 wt% graphite and 5 wt% Nb_2O_5 for 120 min

The similarity between the reaction rates and activation energies of R1 and R3 is rather strange since the addition of Nb_2O_5 to MgH_2 is known to enhance the hydrogenation/de-hydrogenation kinetics via the formation of $MgNb_2O_{3.67}$ at the MgH_2 surface and the grain refinement during ball milling. $MgNb_2O_{3.67}$ provides hydrogen diffusion pathways, which allow a fast hydrogen diffusion through the MgH_2/Mg grains and helps dissociating the hydrogen at the Mg surface.[8, 67-70] Consequently, the achievement of faster hydrogenation/de-hydrogenation reaction kinetics and lower values of de-hydrogenation activation energy was expected for the material milled with Nb_2O_5. A possible explanation for the not achieved improvement of the kinetics rates can be found in the presence of large quantities of graphite into the system. The formation of $MgNb_2O_{3.67}$ together with MgO takes place through the reaction between Nb_2O_5 and Mg/MgH_2. [8, 67-69] Once that Mg is milled with graphite, a graphite coating layer is formed on the surface of the particles.[71, 72] Due to its reducing character, the addition of graphite inhibits the formation of oxide layers on the powders surface and consequently the formation of $MgNb_2O_{3.67}$. [73] This supposition is partially confirmed by the XRD analyses reported in Figure 5 and 7 where no traces of MgO are observed in any of the diffraction patterns of the material milled with Nb_2O_5. However, the presence of nanostructured MgO (therefore not visible in the XRD patterns) cannot be excluded.

In real scale application, the hydrogen storage capacity of the material must be kept constant over several hundreds of hydrogenation/de-hydrogenation cycles. Therefore, the long-term cyclic stability of a system has the same importance as the reaction rates and storage capacity. In this work, due to time and instrumental limitations, the stability of the hydrogen storage capacity over hydrogenation/de-hydrogenation cycling was investigated over 20 hours

for a limited but meaningful number of cycles (Figure 9-11). Based on the Rietveld analysis of as received material (96 wt% Mg and 4 wt% Al) and considering the amount of added graphite and Nb_2O_5 we can assume that the maximum possible hydrogen storage capacity of the investigated material is the following: as-received 7.2 wt%, R1 6.5 wt%, R2 6.8 wt%, R3 6.1 wt%. However, considering that the starting material contains a few weight percent of other elements alloyed but not visible by the XRD analysis (see EDX analysis in Figure S1), the practical hydrogen storage capacity is surely sensibly lower. Therefore, it is not surprising that for none of the investigated materials the expected hydrogen capacity was achieved within the applied measurement time (Figure 6, 9-11). However, for as-received and for R1-20, R1-60, R3-20 and R3-60 samples the main reason for the not achieved hydrogen storage capacity is clearly the rather large particle dimension and the consequent difficulty for hydrogen to reach the Mg particles core once the hydride layer is formed. It is well known that for not doped Mg based systems the hydrogen storage capacity decreases over cycling due the coarsening of the Mg grains, and the interactions with gaseous impurities[70]. Pure magnesium sample shows a significant reduction of hydrogen capacity upon cycling.[74]

Indeed, R1-20 shows a slight but visible decrement of the hydrogen storage capacity after the 4th hydrogenation/de-hydrogenation cycle. Interestingly, the hydrogen storage capacity of R1-60, R1-120, R2-120, R3-20, R3-60 and R3-120 remained constant over the 20 hours cycling. In order to understand if a decrease of the hydrogen storage capacity will take place for a larger number of hydrogenation/de-hydrogenation cycles, we performed a final cycling test on the sample R2-120 (Figure S2). We choose this sample because it shows the highest hydrogen storage capacity among the mixtures investigated in this work. The result of this analysis clearly confirms the fact that differently from the un-doped Mg based materials reported in literature, the obtained material (in this case R2-120) is fully reversible also after more than 70 cycles. To understand the reasons behind the observed reversibility it is necessary to analyze carefully the composition of this alloy. In fact, as observed in the EDX analysis of Figure S1, several well dispersed and nanometric transition metals (TM) particles are also present besides Mg and Al. Once this alloy was stored in air, the TMs likely underwent an oxidation process that led to the formation of TM oxides that, as reported in the literature, are effective catalysts for the hydrogenation/de-hydrogenation process of Mg based systems. In addition, the presence of the well dispersed graphite covering the particle surfaces might prevent deleterious agglomeration phenomena.

Observing with attention the XRD analyses of figure 5, it is possible to see a microstructural peculiarity which occurs during milling of R1 and R3 but that surely is common also to R2 and more in general to all the Mg alloys which undergo ball milling processes after previous mechanical treatment, such as the one that the material used in this work experienced. The diffraction pattern of as received material does not show any preferential orientation of diffraction peaks. However, upon milling it is visible that in the diffraction patterns of R1-20 and R3-20 there is a marked preferential orientation of the 002 plane. The preferential orientation on this plane is still clearly visible after a milling time of 60 minutes (R1-60 and R3-60) and it is sensibly reduced in the diffraction patterns of material milled 120 minutes (R1-120 and R3-120). To better understand this phenomenon we evaluated the crystallite size (Figure 12) and the internal stress (Figure 13) of Mg in the as received material and in the material milled for increasing time (i.e. R1 and R3). The crystallite size and internal stress in the as received material are respectively 29.7 ±1 nm and 0.145 GPa. Surprisingly, for R1-20 the crystallite size increases to 48.2 ±1 nm and internal stress decreases up to 0.03 GPa. For R1-60 the values of crystallite size and internal stress are 45.7 ±1 nm and 0.112 GPa, respectively. For R1-120 these values strongly decrease to 33.1 ±1 nm and 0.004 GPa. The values of crystallite size and internal stress measured for the material milled with Nb_2O_5 (R3) trace out those measured for R1. In fact, the obtained values are 47.5 ±1 nm and 0.03 GPa for R3-20, 44.4 ±1 nm and 0.08 GPa for R3-60 and 32.3 ±1 nm and 0.008 GPa for R3-120.

The observed values of crystallite size and of internal stress measured together with the observed preferential orientation of the planes (002) (Figure 5) in the diffraction pattern for R1 and R3 are most likely consequence of the material history prior the use in this work. Since raw magnesium (as-received material) was obtained from the waste of manufacturing processes, we believe that the particularly small crystallite size observed for the as received material is a consequence of the manufacturing (cutting) procedure. In fact, when a metal undergoes a mechanical treatment at low temperature such as cutting, the most of the energy spent for the plastic deformation is kept into the material as defects (line defects or point defect). When such energy exceeds a certain value, a reorganization of the material microstructure can take place (smaller values of crystallite size and higher values of internal stress). A behavior similar to the one observed in this work (increasing crystallite size after milling) has been reported by R. Floriano [75] for materials that have experienced severe plastic deformation as the consequence of mechanical process prior milling. An acceptable explanation for this phenomenon is the occurrence of recrystallization during ball milling. The

stored energy due to the high number of crystalline defects in the deformed state after severe plastic deformation combined with the local temperature increase during ball milling (and consequent increase of atoms mobility) acts as driving force for the nucleation and growth processes of stress-free Mg grains. However, after the new Mg grains are formed, the further milling leads to a new crystallite size decrement and to oscillating internal stress values while the grains are first decreased in size and newly nucleated subsequently. The evolution of the crystallographic orientation of the planes (002) is a direct consequence of the microstructural re-organization of the material taking place upon milling. A slip plane is the one at which plastic deformation occurs due to the dislocation movement. Magnesium has a hexagonal structure, therefore, there are three possible slip planes at which dislocation movement can take place: i.e. basal, prismatic and pyramidal.[76, 77] In hexagonal structures, the ratio between the c and a dimensions determine the type of slip planes through which plastic deformations occur. Hexagonal structures that have a c/a ratio close to the ideal value (1.63) tends to have the basal plane as the plane responsible for deformations. Interestingly, magnesium has a value of c/a equal to 1.624 therefore close to the ideal one (1.63). Consequently it is obvious that the slip plane responsible for the deformation in magnesium is mainly the basal plane (002) and that is mirrored in the preferential orientation of this plane, visible in the XRD patterns of Figure 5.
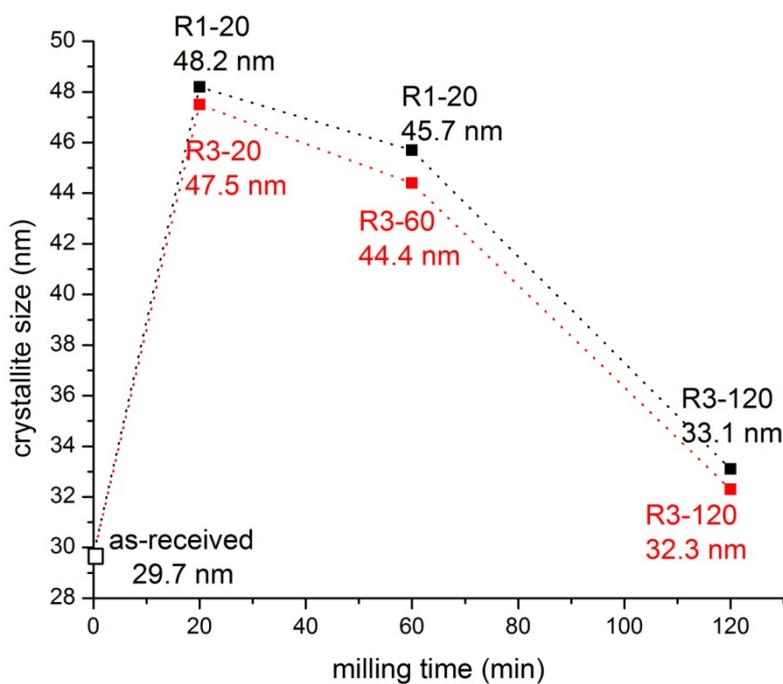

Figure 12. Magnesium crystallite sizes for as-received, R1 and R3 at different milling times.
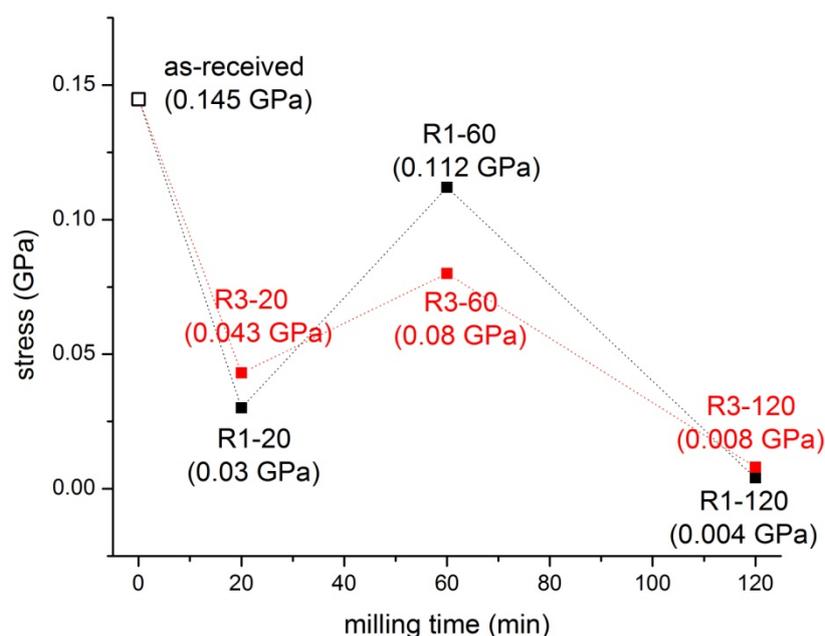
Figure 13. Magnesium internal stress for as-received, R1 and R3 at different milling times.

5. Conclusion

In this work, the possibility to use waste Mg-Al based alloys as starting material for the production of good quality hydrogen storage systems through the use of industrial mills was investigated. Indeed this waste appears suitable for the production of high performance MgH_2. Among the investigates samples, the highest hydrogen sorption capacity (~6 wt%) and the fastest hydrogenation kinetic (26.85% conversion per minute) were achieved by 120 minutes milling a mixture of waste magnesium alloys with 5 wt% graphite in Simoloyer-CM08 ball-mill (R2-120). This sample shows full reversibility even after more than 40 hydrogenation/de-hydrogenation cycles without any meaningful drop of hydrogenation/de-hydrogenation rates. The addition of Nb_2O_5 does not appear to influence/improve the material properties in terms of kinetic behavior and hydrogen storage capacity.

6. Acknowledgements

7. References

[1] Elliott D. A balancing act for renewables. Nature Energy. 2016;1.

[2] Møller KT, Jensen TR, Akiba E, Li HW. Hydrogen - A sustainable energy carrier. Progress in Natural Science: Materials International. 2017;27:34-40.

[3] Hirscher M. Handbook of Hydrogen Storage: Wiley; 2010.

[4] Yu X, Tang Z, Sun D, Ouyang L, Zhu M. Recent advances and remaining challenges of nanostructured materials for hydrogen storage applications. Progress in Materials Science. 2017;88:1-48.

[5] Sakintuna B, Lamari-Darkrim F, Hirscher M. Metal hydride materials for solid hydrogen storage: A review. International Journal of Hydrogen Energy. 2007;32:1121-40.

[6] Deledda S, Borissova A, Poinsignon C, Botta WJ, Dornheim M, Klassen T. H-sorption in MgH2 nanocomposites containing Fe or Ni with fluorine. Journal of Alloys and Compounds. 2005;404-406:409-12.

[7] Friedrichs O, Sánchez-López JC, López-Cartes C, Dornheim M, Klassen T, Bormann R, et al. Chemical and microstructural study of the oxygen passivation behaviour of nanocrystalline Mg and MgH2. Applied Surface Science. 2006;252:2334-45.

[8] Friedrichs O, Sánchez-López JC, López-Cartes C, Klassen T, Bormann R, Fernández A. Nb2O5 "pathway effect" on hydrogen sorption in Mg. Journal of Physical Chemistry B. 2006;110:7845-50.

[9] Huhn PA, Dornheim M, Klassen T, Bormann R. Thermal stability of nanocrystalline magnesium for hydrogen storage. Journal of Alloys and Compounds. 2005;404-406:499-502.

[10] Stander CM. Kinetics of formation of magnesium hydride from magnesium and hydrogen. Zeitschrift Fur Physikalische Chemie-Frankfurt. 1977;104:229-38.

[11] Stander CM. Kinetics of decomposition of magnesium hydride. Journal of Inorganic & Nuclear Chemistry. 1977;39:221-3.

[12] Wiswall R. Topics in Applied Physics, vol29, Hydrogen in Metals 2. 1978:209.

[13] Zaluska A, Zaluski L, Ström-Olsen JO. Nanocrystalline magnesium for hydrogen storage. Journal of Alloys and Compounds. 1999;288:217-25.

[14] Dornheim M, Doppiu S, Barkhordarian G, Boesenberg U, Klassen T, Gutfleisch O, et al. Hydrogen storage in magnesium-based hydrides and hydride composites. Scripta Materialia. 2007;56:841-6.

[15] Korablov D, Ångström J, Ley MB, Sahlberg M, Besenbacher F, Jensen TR. Activation effects during hydrogen release and uptake of MgH2. International Journal of Hydrogen Energy. 2014;39:9888-92.

[16] Khandelwal A, Agresti F, Capurso G, Lo Russo S, Maddalena A, Gialanella S, et al. Pellets of MgH2-based composites as practical material for solid state hydrogen storage. International Journal of Hydrogen Energy. 2010;35:3565-71.

[17] Xia G, Tan Y, Chen X, Sun D, Guo Z, Liu H, et al. Monodisperse Magnesium Hydride Nanoparticles Uniformly Self-Assembled on Graphene. Advanced Materials. 2015;27:5981-8.

[18] Ouyang LZ, Cao ZJ, Wang H, Liu JW, Sun DL, Zhang QA, et al. Dual-tuning effect of In on the thermodynamic and kinetic properties of Mg2Ni dehydrogenation. International Journal of Hydrogen Energy. 2013;38:8881-7.

[19] Cao Z, Ouyang L, Wu Y, Wang H, Liu J, Fang F, et al. Dual-tuning effects of In, Al, and Ti on the thermodynamics and kinetics of Mg85In5Al5Ti5 alloy synthesized by plasma milling. Journal of Alloys and Compounds. 2015;623:354-8.

[20] Ouyang L, Cao Z, Wang H, Hu R, Zhu M. Application of dielectric barrier discharge plasma-assisted milling in energy storage materials – A review. Journal of Alloys and Compounds. 2017;691:422-35.

[21] Ouyang LZ, Cao ZJ, Wang H, Liu JW, Sun DL, Zhang QA, et al. Enhanced dehydriding thermodynamics and kinetics in Mg(In)–MgF2 composite directly synthesized by plasma milling. Journal of Alloys and Compounds. 2014;586:113-7.

[22] Reilly JJ, Wiswall RH. Reaction hydrogen with alloys magnesium and nikel and formation of Mg2NiH4. Inorganic Chemistry. 1968;7:2254-6.

[23] Ouyang LZ, Yang XS, Zhu M, Liu JW, Dong HW, Sun DL, et al. Enhanced Hydrogen Storage Kinetics and Stability by Synergistic Effects of in Situ Formed CeH2.73 and Ni in CeH2.73-MgH2-Ni Nanocomposites. The Journal of Physical Chemistry C. 2014;118:7808-20.

[24] Ouyang LZ, Qin FX, Zhu M. The hydrogen storage behavior of Mg3La and Mg3LaNi0.1. Scripta Materialia. 2006;55:1075-8.

[25] Ouyang LZ, Yang XS, Dong HW, Zhu M. Structure and hydrogen storage properties of Mg3Pr and Mg3PrNi0.1 alloys. Scripta Materialia. 2009;61:339-42.

[26] Zhu M, Wang H, Ouyang LZ, Zeng MQ. Composite structure and hydrogen storage properties in Mg-base alloys. International Journal of Hydrogen Energy. 2006;31:251-7.

[27] Deprez E, Muñoz-Márquez MA, Jimenez de Haro MC, Palomares FJ, Soria F, Dornheim M, et al. Combined x-ray photoelectron spectroscopy and scanning electron microscopy studies of the LiBH4-MgH2 reactive hydride composite with and without a Ti-based additive. Journal of Applied Physics. 2011;109:-.

[28] Garroni S, Milanese C, Girella A, Marini A, Mulas G, Menendez E, et al. Sorption properties of NaBH(4)/MH(2) (M = Mg, Ti) powder systems. International Journal of Hydrogen Energy. 2010;35:5434-41.

[29] Garroni S, Milanese C, Pottmaier D, Mulas G, Nolis P, Girella A, et al. Experimental Evidence of Na-2[B12H12] and Na Formation in the Desorption Pathway of the 2NaBH4 + MgH2 System. Journal of Physical Chemistry C. 2011;115:16664-71.

[30] Garroni S, Minella CB, Pottmaier D, Pistidda C, Milanese C, Marini A, et al. Mechanochemical synthesis of NaBH4 starting from NaH-MgB2 reactive hydride composite system. International Journal of Hydrogen Energy. 2013;38: 2363-9.

[31] Garroni S, Pistidda C, Brunelli M, Vaughan GBM, Surinach S, Baro MD. Hydrogen desorption mechanism of 2NaBH(4) + MgH2 composite prepared by high-energy ball milling. Scripta Materialia. 2009;60:1129-32.

[32] Hu J, Wu G, Liu Y, Xiong Z, Chen P, Murata K, et al. Hydrogen Release from Mg(NH2)2-MgH2 through Mechanochemical Reaction. The Journal of Physical Chemistry B. 2006;110:14688-92.

[33] Jepsen J, Milanese C, Girella A, Lozano GA, Pistidda C, Bellosta Von Colbe JM, et al. Compaction pressure influence on material properties and sorption behaviour of LiBH4-MgH2 composite. International Journal of Hydrogen Energy. 2013;38:8357-66.

[34] Mao JF, Yu XB, Guo ZP, Liu HK, Wu Z, Ni J. Enhanced hydrogen storage performances of NaBH4-MgH2 system. Journal of Alloys and Compounds. 2009;479:619-23.

[35] Minella CB, Pistidda C, Garroni S, Nolis P, Baró MD, Gutfleisch O, et al. Ca(BH4)2 + MgH2: Desorption Reaction and Role of Mg on Its Reversibility. The Journal of Physical Chemistry C. 2013;117:3846-52.

[36] Nwakwuo CC, Pistidda C, Dornheim M, Hutchison JL, Sykes JM. Microstructural study of hydrogen desorption in 2NaBH4 + MgH2 reactive hydride composite. International Journal of Hydrogen Energy. 2012;37:2382-7.

[37] Pottmaier D, Pistidda C, Groppo E, Bordiga S, Spoto G, Dornheim M, et al. Dehydrogenation reactions of 2NaBH4 + MgH2 system. International Journal of Hydrogen Energy. 2011;36:7891-6.

[38] Vajo JJ, Mertens F, Ahn CC, Bowman RC, Fultz B. Altering Hydrogen Storage Properties by Hydride Destabilization through Alloy Formation: LiH and MgH2 Destabilized with Si. The Journal of Physical Chemistry B. 2004;108:13977-83.

[39] Bosenberg U, Doppiu S, Mosegaard L, Barkhordarian G, Eigen N, Borgschulte A, et al. Hydrogen sorption properties of MgH2-LiBH4 composites. Acta Materialia. 2007;55:3951-8.

[40] Bosenberg U, Kim JW, Gosslar D, Eigen N, Jensen TR, von Colbe JMB, et al. Role of additives in LiBH4-MgH2 reactive hydride composites for sorption kinetics. Acta Materialia. 2010;58:3381-9.

[41] Crivello JC, Dam B, Denys RV, Dornheim M, Grant DM, Huot J, et al. Review of magnesium hydride-based materials: development and optimisation. Applied Physics A: Materials Science and Processing. 2016;122:1-20.

[42] Crivello JC, Denys RV, Dornheim M, Felderhoff M, Grant DM, Huot J, et al. Mg-based compounds for hydrogen and energy storage. Applied Physics A: Materials Science and Processing. 2016;122:1-17.

[43] Gosalawit-Utke R, Milanese C, Javadian P, Girella A, Laipple D, Puszkiel J, et al. 2LiBH4-MgH2-0.13TiCl4 confined in nanoporous structure of carbon aerogel scaffold for reversible hydrogen storage. Journal of Alloys and Compounds. 2014;599:78-86.

[44] Gosalawit-Utke R, Thiangviriya S, Javadian P, Laipple D, Pistidda C, Bergemann N, et al. Effective nanoconfinement of 2LiBH4-MgH2 via simply MgH2 premilling for reversible hydrogen storages. International Journal of Hydrogen Energy. 2014;39: 15614-26.

[45] Puszkiel J, Garroni S, Milanese C, Gennari F, Klassen T, Dornheim M, et al. Tetrahydroborates: Development and Potential as Hydrogen Storage Medium. Inorganics. 2017;5:74.

[46] Barkhordarian G, Jensen TR, Doppiu S, Bosenberg U, Borgschulte A, Gremaud R, et al. Formation of Ca(BH4)2 from Hydrogenation of CaH2+MgB2 Composite. The Journal of Physical Chemistry C. 2008;112:2743-9.

[47] Barkhordarian G, Klassen T, Dornheim M, Bormann R. Unexpected kinetic effect of MgB2 in reactive hydride composites containing complex borohydrides. Journal of Alloys and Compounds. 2007;440:L18-L21.

[48] Jepsen J, Bellosta Von Colbe JM, Klassen T, Dornheim M. Economic potential of complex hydrides compared to conventional hydrogen storage systems. International Journal of Hydrogen Energy. 2012;37:4204-14.

[49] Pistidda C, Bergemann N, Wurr J, Rzeszutek A, Møller KT, Hansen BRS, et al. Hydrogen storage systems from waste Mg alloys. Journal of Power Sources. 2014;270:554-63.

[50] NADCA. Product specification standards for die casting. 2009.

[51] Asami K, Ono S. Quantitative X-Ray Photoelectron Spectroscopy Characterization of Magnesium Oxidized in Air. Journal of The Electrochemical Society. 2000;147:1408-13.

[52] Do T, Splinter SJ, Chen C, McIntyre NS. The oxidation kinetics of Mg and Al surfaces studied by AES and XPS. Surface Science. 1997;387:192-8.

[53] Feliu Jr S, Maffiotte C, Galván JC, Barranco V. Atmospheric corrosion of magnesium alloys AZ31 and AZ61 under continuous condensation conditions. Corrosion Science. 2011;53:1865-72.

[54] Feliu Jr S, Maffiotte C, Samaniego A, Galván JC, Barranco V. Effect of naturally formed oxide films and other variables in the early stages of Mg-alloy corrosion in NaCl solution. Electrochimica Acta. 2011;56:4554-65.

[55] Feliu Jr S, Pardo A, Merino MC, Arrabal R, Matykina E. XPS study of chemical changes on the La/Ce treated surface of A361 aluminium alloy exposed to air at temperatures up to 500 °c. Advances in Materials Science and Engineering. 2009;2009.

[56] Feliu Jr S, Pardo A, Merino MC, Coy AE, Viejo F, Arrabal R. Correlation between the surface chemistry and the atmospheric corrosion of AZ31, AZ80 and AZ91D magnesium alloys. Applied Surface Science. 2009;255:4102-8.

[57] Feliu Jr S, Samaniego A, Bermudez EA, El-Hadad AA, Llorente I, Galván JC. Effect of native oxide film on commercial magnesium alloys substrates and carbonate conversion coating growth and corrosion resistance. Materials. 2014;7:2534-60.

[58] Fuggle JC, Watson LM, Fabian DJ, Affrossman S. X-ray photoelectron studies of the reaction of clean metals (Mg, Al, Cr, Mn) with oxygen and water vapour. Surface Science. 1975;49:61-76.

[59] McIntyre NS, Chen C. Role of impurities on Mg surfaces under ambient exposure conditions. Corrosion Science. 1998;40:1697-709.

[60] Santamaria M, Di Quarto F, Zanna S, Marcus P. Initial surface film on magnesium metal: A characterization by X-ray photoelectron spectroscopy (XPS) and photocurrent spectroscopy (PCS). Electrochimica Acta. 2007;53:1314-24.

[61] Splinter SJ, McIntyre NS, Lennard WN, Griffiths K, Palumbo G. An AES and XPS study of the initial oxidation of polycrystalline magnesium with water vapour at room temperature. Surface Science. 1993;292:130-44.

[62] Varin RA, Czujko T, Wronski Z. Particle size, grain size and γ-MgH2 effects on the desorption properties of nanocrystalline commercial magnesium hydride processed by controlled mechanical milling. Nanotechnology. 2006;17:3856-65.

[63] Pasquini L, Callini E, Piscopiello E, Montone A, Antisari MV, Bonetti E. Metal-hydride transformation kinetics in Mg nanoparticles. Applied Physics Letters. 2009;94.

[64] Suryanarayana C. Mechanical alloying and milling. Progress in Materials Science. 2001;46:1-184.

[65] Campostrini R, Abdellatief M, Leoni M, Scardi P. Activation energy in the thermal decomposition of MgH2 powders by coupled TG-MS measurements: Part II. Catalytic effects of tin oxide doping. Journal of Thermal Analysis and Calorimetry. 2014;116:865-74.

[66] Schulz R, Huot J, Liang G, Boily S, Lalande G, Denis MC, et al. Recent developments in the applications of nanocrystalline materials to hydrogen technologies. Materials Science and Engineering A. 1999;267:240-5.

[67] Dolci F, Di Chio M, Baricco M, Giamello E. Niobium pentoxide as promoter in the mixed MgH2/Nb 2O5 system for hydrogen storage: A multitechnique investigation of the H2 uptake. Journal of Materials Science. 2007;42:7180-5.

[68] Friedrichs O, Aguey-Zinsou F, Fernández JRA, Sánchez-López JC, Justo A, Klassen T, et al. MgH2 with Nb2O5 as additive, for hydrogen storage: Chemical, structural and kinetic behavior with heating. Acta Materialia. 2006;54:105-10.

[69] Friedrichs O, Klassen T, Sánchez-López JC, Bormann R, Fernández A. Hydrogen sorption improvement of nanocrystalline MgH2 by Nb2O5 nanoparticles. Scripta Materialia. 2006;54:1293-7.

[70] Dornheim M, Eigen N, Barkhordarian G, Klassen T, Bormann R. Tailoring Hydrogen Storage Materials Towards Application. Advanced Engineering Materials. 2006;8:377-85.

[71] Mikhailova SS, Lakhnik AM, Gil'mutdinov FZ, Karban OV, Rud AD, Lad'yanov VI. Structure and surface layers of Mg-C nanocomposites produced by ball milling. Bulletin of the Russian Academy of Sciences: Physics. 2011;75:1462-7.

[72] Rud AD, Lakhnik AM, Mikhailova SS, Karban OV, Surnin DV, Gilmutdinov FZ. Structure of Mg-C nanocomposites produced by mechano-chemical synthesis. Journal of Alloys and Compounds. 2011;509:S592-S4.

[73] Milanese C, Girella A, Garroni S, Bruni G, Berbenni V, Matteazzi P, et al. Effect of C (graphite) doping on the H2 sorption performance of the Mg-Ni storage system. International Journal of Hydrogen Energy. 2010;35:1285-95.

[74] Ponthieu M, Calizzi M, Pasquini L, Fernández JF, Cuevas F. Synthesis by reactive ball milling and cycling properties of MgH2–TiH2 nanocomposites: Kinetics and isotopic effects. International Journal of Hydrogen Energy. 2014;39:9918-23.

[75] Floriano R, Leiva DR, Deledda S, Hauback BC, Botta WJ. Nanostructured MgH2 obtained by cold rolling combined with short-time high-energy ball milling. Materials Research. 2013;16:158-63.

[76] Wang H, Wu PD, Boyle KP, Neale KW. On crystal plasticity formability analysis for magnesium alloy sheets. International Journal of Solids and Structures. 2011;48:1000-10.

[77] Wang YN, Huang JC. Transition of dominant diffusion process during superplastic deformation in AZ61 magnesium alloys. Metallurgical and Materials Transactions A: Physical Metallurgy and Materials Science. 2004;35 A:555-62.